Solvent Effects in the Adsorption of Alkyl Thiols on Gold Structures: A Molecular Simulation Study

ARTICLE *in* THE JOURNAL OF PHYSICAL CHEMISTRY C · JULY 2007

Impact Factor: 4.77 · DOI: 10.1021/jp071491d · Source: OAI

3 AUTHORS, INCLUDING:

René Pool
VU University Amsterdam
24 PUBLICATIONS **466** CITATIONS
SEE PROFILE

Philipp Schapotschnikow
Brains for hire
12 PUBLICATIONS **366** CITATIONS
SEE PROFILE

Solvent Effects in the Adsorption of Alkyl Thiols on Gold Structures: A Molecular Simulation Study

René Pool, Philipp Schapotschnikow, and Thijs J. H. Vlugt*

Condensed Matter and Interfaces, Utrecht University, P.O. Box 80000, 3508 TA Utrecht, The Netherlands

Received: February 22, 2007; In Final Form: April 27, 2007

We carried out Monte Carlo simulations of gold nanocrystals (NCs) and (111) slabs covered with alkyl thiols, with and without explicit solvent (*n*-hexane), at $T = 300$ K. Adsorption isotherms for propane- and octanethiol showed a phase behavior measured previously in experiments. Comparison of the adsorption isotherm of octanethiol in hexane on a (111) slab with experimental data suggests that, in this system, no thiolate bond was formed. The geometry of a gold surface strongly influences the formation and structure of the capping monolayer. On a (111) surface, attractive interactions between carbon chains are more pronounced than on a NC. This leads to a stronger penetration of the capping layer by the solvent. Adsorption selectivity for binary alkyl thiol mixtures is stronger in vacuum than in solution. The convex shape of the NCs also reduces the adsorption selectivity of binary thiol mixtures. This result shows that the solvent cannot be ignored in simulations.

1. Introduction

Nanometer-sized materials are of growing importance in the fields of optics, electronics, catalysis, ceramics, magnetic storage, and biophysics. Gold and semiconductor nanocrystals (NCs) with specific size- and shape-dependent optical and electrical behavior constitute an important class of such materials. These NCs can self-assemble in a range of different 2D and 3D superstructures.[1−3]

NCs are often protected by an organic capping layer of surfactants that prevents aggregation;[4] for example, gold NCs are often capped with alkyl thiol molecules.[5−8] Furthermore, adding surfactants during colloidal synthesis allows for control of the size and shape of the formed NCs.[9−11] On planar gold surfaces, alkyl thiols are known to form well-organized structures called self-assembled monolayers (SAMs). The gold−thiol interaction is very strong, preventing the surfactants from evaporating or dissolving. As a result, these SAMs are stable at ambient conditions. Gold SAM structures are promising for various applications such as controlled wetting, catalysis, sensoring, and in biotechnology.[12,13] A large amount of research has been carried out on the preparation, structure, and application of SAMs of alkyl thiols on gold. For two reasons, gold (111) surfaces are often studied; they are easy to prepare experimentally,[13] and thiols adsorb readily on such surfaces.[14] Thiol heads preferably adsorb on hollow sides between 3 Au atoms and form a 2D hexagonal overlattice on the flat (111) surface with S−S spacing of ≈5 Å. On saturated systems, the aliphatic tails align parallel to each other, making an angle of 25−30° with the surface normal.[12] Less is known about the formation of SAMs and the structure of unsaturated systems. Poirier et al. described a coverage-dependent transition from a 2D liquid to a 2D crystal during the formation of the butanethiol SAM[15] without the presence of a solvent. For decanethiol, even more coverage-dependent 2D-phases are possible.[16] This in contrast to the Langmuir adsorption behavior for octanethiol in *n*-hexane solution, observed by Karpovich and Blanchard.[17]

While self-assembled monolayers of alkyl thiols have been studied extensively, less is known about the structure of these molecules adsorbed on gold NCs. At room temperature, octanethiol and shorter thiols are completely conformationally disordered.[5] Experiments show that temperature-induced phase transitions of the capping layer of CdSe NCs dramatically alter optical properties of NCs in solution.[18] This is due to the reconstruction of the NC surface, induced by phase transitions in the capping layer. Therefore, it is of considerable importance to study how the internal structure of molecules in the capping layer depends on the geometry (size, shape, and curvature) of NCs. It was also observed that the structure of 2D and 3D assemblies of NCs strongly depends on the nature of the surfactant molecules and the solvent and also on the NC size.[6,7,19]

As it is difficult to obtain such structural data or information on the adsorption behavior on NCs from experiments, molecular simulations may provide more insight on this topic. Several molecular simulation studies on gold−thiolate systems have been undertaken. Hautman and Klein developed the first effective potential for the gold (111)−sulfur and gold (111)−carbon interactions.[20] They mimicked gold as a plane without structure interacting with united atoms. This model was quickly adopted because it correctly describes the structure of SAMs.[20,21] Furthermore, using the effective potential is computationally relatively cheap compared to full Au atom models. In refs 22−24, the Hautman-Klein model was used to describe phase behavior of mixed SAMs using MC, while refs 25 and 26 used lattice models. In two independent studies,[27,28] atomistic force fields for the Au−thiolate interactions were developed. These were based on ab initio[29] calculations and experimental data[30] on Au−thiolate systems. Several experimentally observed phenomena could be reproduced in molecular dynamics simulations, such as the chain melting temperature of a capping layer and the dependence of the structure of a NC superlattice on the chain length of the capping molecules.[28,31]

In this work, we consider both flat Au(111) surfaces and NCs as sorbates for alkyl thiols. We compute adsorption isotherms to understand the thermodynamics and structural properties involved in the formation of SAMs and capping layers. We will also extend our preliminary simulations[32] for the adsorption selectivities of binary mixtures of alkyl thiols that differ in tail

* To whom correspondence should be addressed. E-mail: t.j.h.vlugt@phys.uu.nl.

10.1021/jp071491d CCC: $37.00
Published on Web 06/14/2007

length to larger NCs. An important aspect in these simulations is the influence of the solvent, which we simulate explicitly. Our aim is to understand the difference between (1) systems in solution and in vacuum and (2) the formation and structure of capping layers on planar Au(111) surfaces and on gold NCs. We found that the solvent significantly reduces the adsorption selectivity for thiol mixtures on NCs.

Previously, saturated alkyl thiol SAMs and capping layers on gold NCs were studied using molecular simulations. In these studies, the Au−S interaction strength is of minor importance. In this work, however, we focus on the actual formation of SAMs and NC capping layers using equilibrium Monte Carlo simulations. Here, the Au−S interaction plays a crucial role. Morse potentials used in refs 28 and 33 yield an almost twice as strong effective interaction compared to the Hautman−Klein potential. We show that as long as the Au−S interaction is, by orders of magnitude, stronger than thermal fluctuations and CH_x-CH_y and $Au-CH_x$ interactions, the results from different adsorption simulations can be related by a simple mathematical transformation.

The paper is structured as follows. We present our model and simulation method in sections 2 and 3, respectively. In section 4.1, adsorption isotherms are presented and discussed. We will also focus on the structural properties of adsorbed system at various loadings, such as orientation and density profiles. In section 4.2, we investigate selective adsorption of binary mixtures of alkyl thiols with different chain lengths. In Appendix A, we explain why and how results from simulations with different Au−S interaction models can be related. In Appendix B, we briefly describe the biased insertion technique used in our simulations.

2. Model

We apply a united atom model where groups of atoms are represented by single pseudoatoms. We use this approach for SH, CH_2, and CH_3. We denote the first by S and the last two by C (a C segment at the end of a chain is a CH_3 type and a CH_2 type otherwise). We name the surfactants (alkyl thiols) "SC*x*", where *x* is the number of alkyl chain segments in the linear tail. Solvent and surfactant molecules interact with each other via truncated and shifted Lennard-Jones (LJ) pair interactions between united atoms

$$\phi_{TS}(r_{ij}) = \begin{cases} \phi_{LJ}(r_{ij}) - \phi_{LJ}(r_c) & r_{ij} \le r_c \\ 0 & r_{ij} > r_c \end{cases} \quad (1)$$

where ϕ_{LJ} is the LJ potential

$$\phi_{LJ}(r_{ij}) = 4\epsilon_{ij}\left[\left(\frac{\sigma_{ij}}{r_{ij}}\right)^{12} - \left(\frac{\sigma_{ij}}{r_{ij}}\right)^{6}\right] \quad (2)$$

In the above equations, r_{ij} is the distance between two united atoms i and j, respectively, and r_c is the cutoff distance (here, $r_c = 12.0$Å). The potential well depth is ϵ_{ij}, and σ_{ij} gives the interaction range for particles i and j. We account for intramolecular bond stretching, bond bending, and torsional forces. Additionally, we apply a LJ interaction between segments that are separated by more than three bonds. For more details, we refer the reader to ref 32. The gold structures are made up from Au atoms that interact with other species via truncated and shifted LJ pair interactions (using $r_c = 12.0$Å). To keep computational efforts to acceptable levels, all gold structures are considered as rigid.

2.1. Au−S and Au−C Interactions. The popular approach by Hautman and Klein[20] of approximating the Au(111) surface−system interaction by a unidirectional effective potential is unsuitable for gold NCs as they typically have an icosahedral shape.[34−36] To make a fair comparison between the adsorption of alkyl thiols on NCs and on flat Au(111) surfaces, interactions with all gold atoms are considered. To derive the parameters for these pair interactions, we start from the Hautman−Klein potential

$$V_{eff}(z) = \frac{C_{12}}{(z - z_0)^{12}} - \frac{C_3}{(z - z_0)^3} \quad (3)$$

where *z* represents the distance of a united atom to the gold surface, and C_{12}, C_3, and z_0 are parameters that determine the potential well depth U_m and its position z_m. We assume that Au atoms interact with other species via a truncated and shifted LJ potential (eq 1). We find the LJ parameters ϵ and σ such that it reproduces $V_{eff}(z)$ by calculating the average interaction energy $\langle U\rangle(z)$ as a function of separation *z* of a single CH_x or S segment from a sufficiently large gold (111) slab with a lattice spacing of 4.08Å. The average interaction at a given separation *z* is determined by randomly generating a large number *N* of x_i, y_i ($i = 1, ..., N$) positions in a plane at distance *z* and calculating the Boltzmann average energy

$$\langle U\rangle(z) = \frac{\sum_{i=1}^{N} \mathcal{I}(z, x_i, y_i) \exp[-\beta \mathcal{I}(z, x_i, y_i)]}{\sum_{i=1}^{N} \exp[-\beta \mathcal{I}(z, x_i, y_i)]} \quad (4)$$

$\mathcal{I}(z, x_i, y_i)$ is the effective interaction with the gold slab, given by

$$\mathcal{I}(z, x_i, y_i) = \sum_{j=1}^{N_{Au}} \phi_{TS}(r_{ij}) \quad (5)$$

where N_{Au} is the number of gold atoms in the slab. A fit of $\langle U\rangle(z)$ to $V^{eff}(z)$ now determines the LJ parameters for the Au−S and Au−C interactions. We consider two cases, one where we compute $\langle U\rangle(z)$ for the desired temperature $T = 300$ K and another where the effective interaction is calculated for the limit $\beta \to 0$ ($T \to \infty$).

For both cases, we found force field parameters that closely reproduce $V^{eff}(z)$ (Table 1). At $T = 300$ K, the Boltzmann weights of the *x*, *y* positions on the plane that are just above a hollow site between three Au atoms of the Au(111) plane have a larger contribution to the average energy $\langle U\rangle(z)$. At $T \to \infty$, all *x*, *y* positions have equal weights in eq 4. As a result, $\epsilon_{T=300K}$ is lower than $\epsilon_{T\to\infty}$; see Table 1. Lowering ϵ leads to a decrease in the effective interaction range as a function of *z*. Hence, a fit to the Hautman−Klein effective potential for $T = 300$ K requires a larger σ parameter compared to that for $T \to \infty$. The force field parameters for each interaction type within our system are summarized in Table 1.

3. Monte Carlo Simulations

To study the adsorption of alkyl thiols on gold (with or without explicit solvent), we apply configurational-bias Monte Carlo (CBMC) simulations.[38−41] During the simulations, the following MC trial moves are used: molecular translations,[42] molecular rotations,[43] (partial) chain regrows, chain insertions/

TABLE 1: Force Field Parameters for the LJ Interactions in Our System[a]

ϵ_{ij}/k_B[K]	CH_3	CH_2	SH	$Au_{T\to\infty}$	$Au_{T=300K}$
CH_3	108	78	117	108	108
CH_2	78	56	84	88	88
SH	117	84	126	4260	2795
$Au_{T\to\infty}$	108	88	4260		
$Au_{T=300K}$	108	88	2795		

σ_{ij}[Å]	CH_3	CH_2	SH	$Au_{T\to\infty}$	$Au_{T=300K}$
CH_3	3.76	3.86	4.11	3.54	3.54
CH_2	3.86	3.96	4.21	3.54	3.54
SH	4.11	4.21	4.45	2.40	2.65
$Au_{T\to\infty}$	3.54	3.54	2.40		
$Au_{T=300K}$	3.54	3.54	2.65		

[a] The CH_x-CH_y interaction parameters are taken from ref 37. The $S-CH_x$ were taken from ref 20. Au−S and $Au-CH_x$ interactions were derived using eqs 4 and 5. Note that the Au structures are rigid, and therefore, we do not include Au−Au interactions.

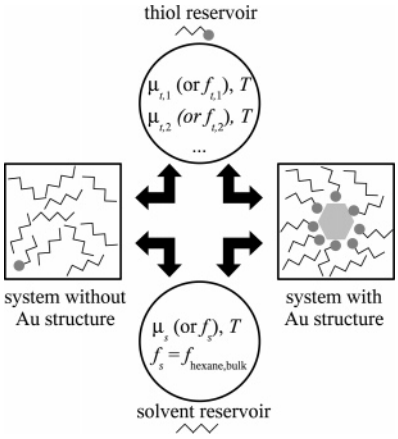

Figure 1. General scheme for the type of simulations performed in this work. We have two reservoirs with which we exchange molecules. By tuning the fugacity $f_{t,i}$ of each thiol, we determine the average number of thiols $\langle N\rangle$ in the system with a gold structure (NC or (111) slab) and in the system without a gold structure present. Due to the very attractive Au−S interaction, the values of $\langle N\rangle$ will not be identical for these systems. To estimate the adsorption isotherm as a function of bulk thiol concentration (c_t, for systems with a solvent present) or thiol density (ρ_t, for systems without a solvent), it is therefore necessary to simulate both systems. For systems with a solvent (*n*-hexane) present, the fugacity, $f_s = 20.0$ kPa, of the solvent is set such that it reproduces the experimental density of pure *n*-hexane at $T = 300$ K.

removals (grand-canonical MC), and identity changes[44] (semi-grand-canonical MC[45]); see Figure 1. For more details, we refer the reader to ref 32. Note that the Au−S interaction is strongly attractive compared to the other intermolecular interactions ($Au-CH_x$, $S-CH_x$, and CH_x-CH_y). This high adsorption affinity requires special insertion techniques to sample the number of adsorbed thiol molecules $\langle N\rangle$ in grand-canonical Monte Carlo simulations (see Appendix B). Sampling efficiency is further improved by artificially weakening the Au−S interaction. In Appendix A, we will show that the precise value of ϵ_{Au-S} is not important and that isotherms can be rescaled for other values of ϵ_{Au-S}.

In Figure 1, we have sketched our simulation setup. We simulate systems either with or without a gold structure. In grand-canonical MC, both systems are allowed to exchange molecules with the solvent reservoir and/or the thiol reservoir. Semi-grand-canonical MC moves can be viewed as removal of a molecule of one type and insertion of another type, with their difference in chemical potential or fugacity ratio as a driving force.

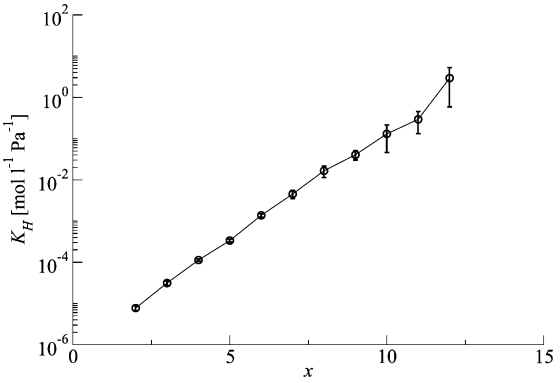

Figure 2. Henry's law coefficients K_H as a function of chain length x of alkyl thiols SCx in hexane at $T = 300$ K.

The simulations of the planar Au(111) systems are performed in rectangular simulation boxes in which a gold slab of $N_{Au,x} \times N_{Au,y} \times N_{Au,z} = 12 \times 12 \times 6$ is oriented parallel to the *xy* plane and situated at half of the box length in the *z* direction. Periodic boundary conditions are applied. We make sure that molecules cannot interact with each other through the slab, that is, molecules on one side of the slab cannot "feel" others on the other side of the slab. The simulations of NCs (consisting of 561 or 1415 Au atoms, with a size of 2.5 and 3.0 nm, respectively) are performed in cubic simulation boxes. For both the simulations of the gold slab as well as simulations with a gold NC, we choose sufficiently large box sizes to avoid interactions between periodic images of the (capped) gold structures. To determine the adsorption isotherms, we calculate the number of alkyl thiols $\langle N\rangle$ adsorbed on the gold structure as a function of the thiol concentration (c_t, for systems with a solvent present) or thiol density (ρ_t, for systems without a solvent) in the other simulation box at the same fugacity of the thiol molecules; see Figure 1.

In all simulations with explicit solvent (*n*-hexane), we impose a solvent fugacity of $f_s = 20.0$ kPa, corresponding to the experimental *n*-hexane density (7.598 mol/L[46] at $T = 300$ K). As the thiol concentration c_t in the box not containing the gold structure is very low, we can use Henry's law $c_t = K_H f_t$ to determine c_t for a given thiol fugacity f_t. We determine the Henry coefficient K_H via (semi)-grand-canonical MC simulations by imposing a thiol fugacity f_t that results in a very low thiol concentration. Figure 2 shows the Henry coefficient K_H as a function of tail length x. As expected, there is a linear relation between ln K_H and tail length x.

For simulations without solvent, the thiol density ρ_t follows directly from the ideal gas law ($f_t = \rho_t k_B T$).

4. Results and Discussion

4.1. Adsorption of Alkyl Thiols to Au NCs and to Au(111) Surfaces. In this section, we present simulation results on the adsorption behavior of alkyl thiols on flat Au surfaces and on Au NCs. We considered two thiol types, SC3 and SC8. To determine the effect of the solvent, we computed adsorption isotherms with and without solvent (vacuum).

4.1.1. Adsorption of SC3 and SC8 in Vacuum. By imposing varying surfactant fugacities in separate grand-canonical MC simulations, we determined adsorption isotherms for SC3 and SC8 thiols on Au_{561} NCs and on flat Au(111) surfaces at $T = 300$ K. For these types of simulations, we only switched on the thiol reservoir in Figure 1. For both gold systems, we present data where we used $\epsilon/k_B = 2795$ K and $\sigma = 2.65$ Å for the LJ interaction between Au and S.

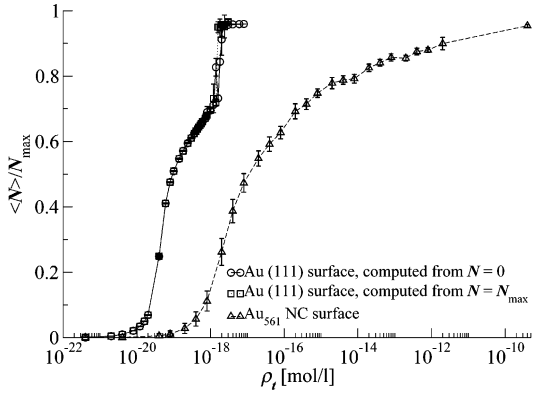

Figure 3. Adsorption isotherms for SC3 on a flat Au(111) surface and on a Au_{561} NC in vacuum at $T = 300$ K. LJ parameters for the Au−S interaction are $\epsilon/k_B = 2795$ K and $\sigma = 2.65$ Å.

We start the discussion with the SC3 thiol. Comparing the flat surface isotherm to the one for a NC (Figure 3), we see that adsorption at the (111) surface starts at lower thiol concentrations and that the transition to the fully loaded surface as a function of ρ_t is much sharper. The first observation is a consequence of the edged nature of the NC surface and the relatively small (111) facets. Therefore, the effective surface−thiol interaction for NCs is lower than that for flat Au(111), and therefore, thiol adsorption starts at a higher ρ_t for NCs. The slower transition to the maximum loading N_{max} on a NC also is a result of its convex shape. Between adsorbed alkyl thiols on flat Au(111), the thiol carbon tails interact favorably with each other, while on the NC surface, these interactions cannot be maintained over the entire surface due to the curvature of the NC. The favorable mutual tail−tail interactions lead to an extra driving force for thiol adsorption and thus make the adsorption isotherm steeper.

For the flat Au(111) surface systems, there is a considerable amount of hysteresis between adsorption isotherms computed starting from fully loaded ($N = N_{max}$) surfaces and from empty ($N = 0$) surfaces (see Figure 4 where we plotted the isotherms on a linear *x*-axis scale). This points to a first-order transition from a 2D liquid to a 2D crystal phase, already observed in experiments.[15] In the crystal phase, sulfur atoms form a well-ordered hexagonal overlattice with a S−S spacing of ≈5 Å, and aliphatic chains stand almost upright and aligned; see Figure 5. In the liquid phase, thiol heads arrange without a pattern, and carbon chains lie closer to the surface; see Figure 6. Both phenomena are in good agreement with experimental observations on self-assembled monolayers of thiols on Au(111).[12]

To illustrate the sampling difficulties around the transition point, we plotted the number of adsorbed thiols as a function of the number of MC cycles in Figure 4 (center). As nucleation and melting are spontaneous events and simulation time is limited, most of the time, the system resides in one of the (meta)-stable states[47] that are separated by sharp transitions. We did not observe this hysteresis loop in the NC isotherms. Again, this is a result of the convex shape of the Au NC.

We also computed the adsorption isotherm of SC3 for an infinitely smooth, flat gold surface in vacuum using the Hautman−Klein potential.[20] As expected, these isotherms have a similar concentration range where thiol adsorption takes place, compared to the explicit atom case (compare Figure 3 to the bottom panel of Figure 4). In the infinitely smooth Au surface system, the 2D liquid phase is more stable than that for the explicit atom system (see Figure 4, top and bottom), and the height of the jump in coverage around phase transition to the

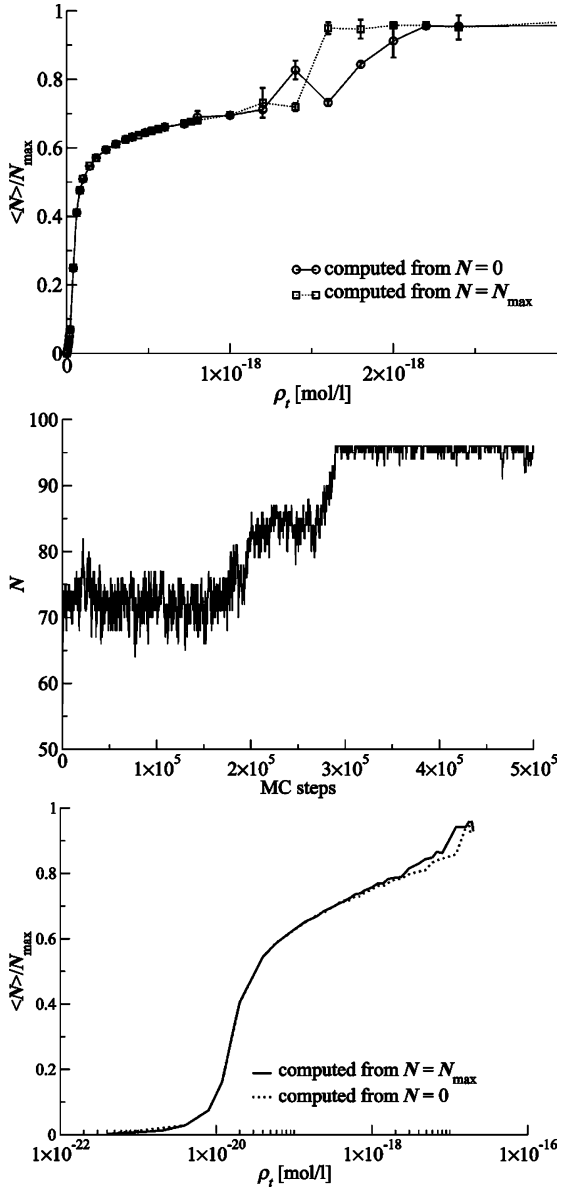

Figure 4. Top: adsorption isotherm for SC3 on a gold (111) surface with explicit atoms in vacuum, computed by increasing and decreasing the loading. Center: typical GCMC behavior around the transition point for a simulation starting from a low coverage. The first terrace corresponds to a 2D liquid phase, then, a phase transition occurs on one of the sides of the slab (second terrace, fictive state due to simulation conditions), and finally, the thiols 2D-crystallize on the second side (third terrace). Bottom: adsorption isotherm for SC3 to an infinitely smooth gold (111) surface in vacuum using the Hautman−Klein potential, computed by increasing and decreasing the loading. All plots are for $T = 300$ K.

2D solid is smaller. Obviously, a 2D liquid can be compressed much more on a infinitely smooth surface than on a rough surface with explicit atoms.

Comparing the SC8 isotherms (Figure 7) to the SC3 ones (Figure 3), we observe that adsorption of the longer-chain thiol starts at lower densities than that for shorter-chain thiols. This is due to the larger number of attractive Au−CH_x interactions for SC8. Comparing the NC SC8 isotherm to the flat (111) surface SC8 isotherm, we again see that adsorption for the flat surface starts at lower concentrations than that for the NC and that the concentration range where adsorption takes place is much narrower for the flat surface system. This is explained by the same arguments as those for SC3.

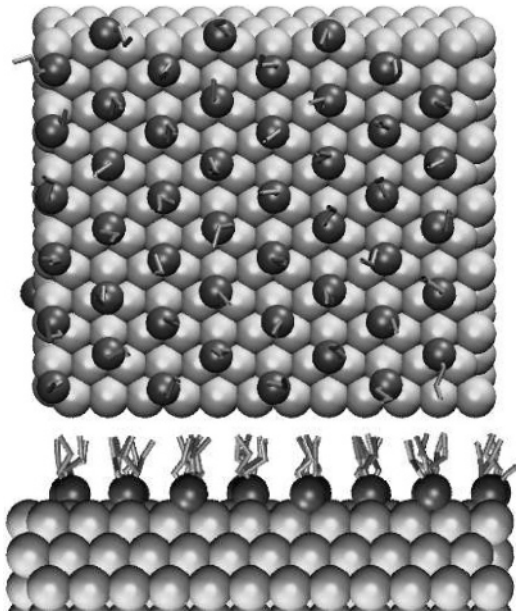

Figure 5. SC3 on Au in the 2D crystal phase. Gold atoms are represented as large light balls, thiol heads as small dark balls, and carbon chains as thin lines. Top: top view. Bottom: side view. Note that the sulfur atoms are highly organized.

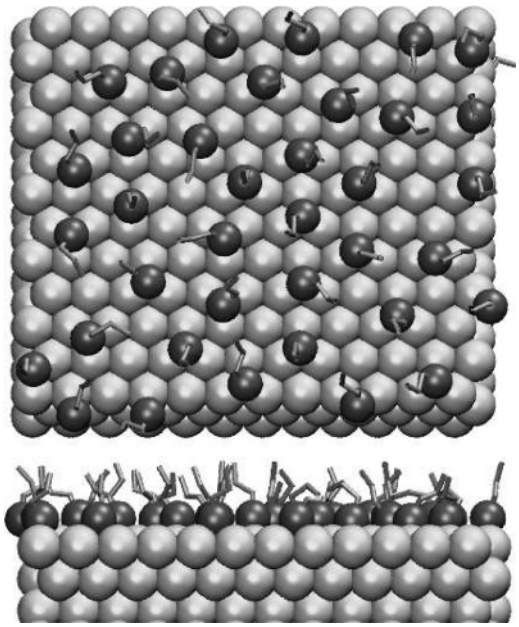

Figure 6. SC3 on Au in the 2D liquid phase. Gold atoms are represented as large light balls, thiol heads as small dark balls, and carbon chains as thin lines. Top: top view. Bottom: side view. Note that the sulfur atoms do not show a clear structure.

The phase behavior of SC8 on flat surfaces is more complicated compared to SC3 (or to the NC case); see Figure 7. We observe two jumps in the isotherm. During the second jump, the coverage doubles. At this point, the self-assembled monolayer is formed. At lower loadings, various 2D phases are formed due to different packing of alkyl chains on the surface.[16] The 2D liquid phase is metastable for long-chain thiols in vacuum. Again, such phase transitions are not present in the NC systems we studied.

4.1.2. Adsorption of SC3 and SC8 in Hexane Solution. Using (semi)-grand-canonical Monte Carlo (GCMC), we computed adsorption isotherms for the alkyl thiols SC3 and SC8 on a Au_{561} NC as well as on a Au(111) surface with explicit solvent (*n*-hexane). This means that both the solvent and the thiol reservoirs

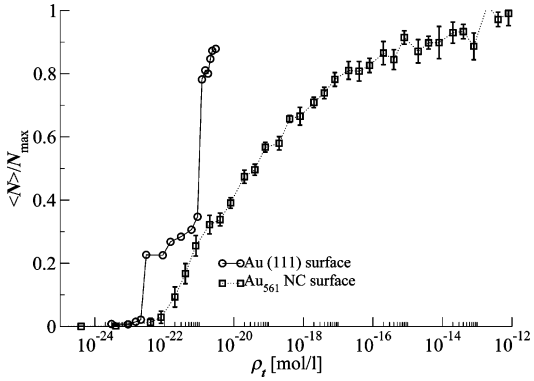

Figure 7. Adsorption isotherm for SC8 on a flat Au(111) surface and on a Au_{561} NC in vacuum at $T = 300$ K.

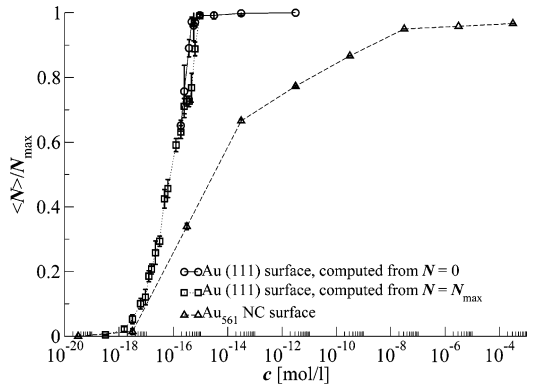

Figure 8. Adsorption isotherm for SC3 on a flat Au(111) surface and on a Au_{561} NC in *n*-hexane at $T = 300$ K.

(Figure 1) were switched on. Again, for both systems, we used $\epsilon/k_B = 2795$ K and $\sigma = 2.65$ Å for the LJ interaction between Au and S.

The SC3 isotherms for the flat Au(111) surface and for the NC are shown in Figure 8. We again observe that adsorption of SC3 on the Au(111) surface starts at a lower c_t than that on the NC. Similar to the vacuum case, the concentration range of adsorption is considerably larger in NC systems compared to that for flat gold systems. Explanations for both are given in the previous subsection. The flat Au(111) SC3 system in explicit solvent also shows the hysteresis loop at high $\langle N \rangle$, pointing to a phase transition from a 2D liquid to a 2D solid, already described above for the vacuum case.

There are, however, differences between SC3 systems with or without solvent. For both the NC and the flat surface, the isotherm is shifted toward higher thiol concentrations. We explain this by a competition effect between the adsorption of solvent and thiols to gold. The shift is moderate because hexane−gold interactions are far weaker than thiol−gold interactions.

An illustration of this competition effect is the difference in the adsorption behavior at low ρ_t between vacuum SC3 systems and those with explicit solvent. In agreement with experiments,[17] the explicit solvent isotherm can be fitted to a Langmuir adsorption isotherm, whereas this is not possible for the vacuum isotherms (see Figure 9). At low loadings, the vacuum isotherm increases superlinearly (i.e., $d^2\langle N \rangle/d\rho_t^2 > 0$; see Figure 9, bottom), while the Langmuir isotherm behaves sublinearly ($d^2\langle N \rangle/d\rho_t^2 < 0$). This difference can be explained as follows. At low loadings in vacuum, alkyl thiols gain energy from the attractive interactions between tails, hence, the superlinear increase of the isotherm. In hexane solution, energetic gains from surfactant tail−tail interactions are accompanied by energy

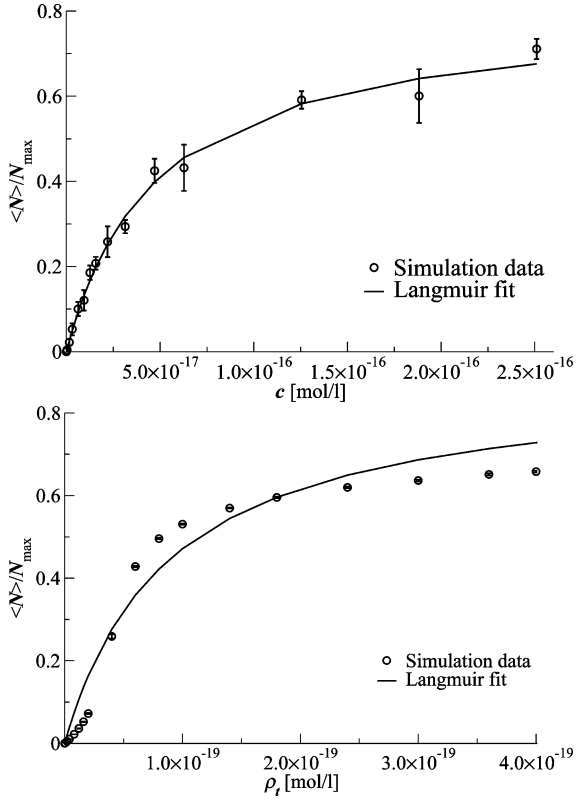

Figure 9. Langmuir fit to the lower part of the adsorption isotherm of SC3 on a gold slab in hexane (top) and vacuum (bottom).

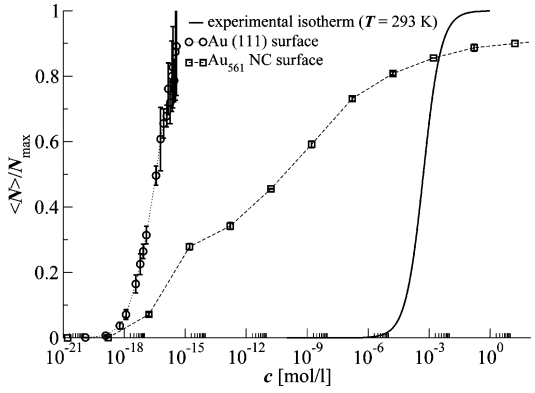

Figure 10. Adsorption isotherm for SC8 on a flat Au(111) surface and on a Au_{561} NC in *n*-hexane at $T = 300$ K, compared to the experimental SC8 isotherm on Au(111) in *n*-hexane[17] (recorded at $T = 293$ K). Note the large shift in adsorption concentration range between the simulated and the experimental isotherm using isotherm shifting (cf. Appendix A). The experimental interaction strength corresponds to $\epsilon/k_B \approx 1000$ K, a factor of 3 lower than the value used in the simulations.

penalties associated with the loss of solvent−solvent and solvent−surfactant interactions. Thus, effectively, the favorable surfactant tail−tail interactions play a less pronounced role in the explicit solvent systems, and therefore, the alkyl thiol adsorption isotherm shows Langmuir behavior.

For adsorption of SC8, the solvent effect, or equivalently the shift of the isotherm when including *n*-hexane as a solvent, is more strongly pronounced (compare Figures 7 to 10). If we compare Figure 7 to Figure 10, we see that various 2D phases[16] disappear in the explicit solvent system, and the 2D liquid phase is stable in contrast to the vacuum case. In Figure 10, we included the SC8/*n*-hexane/Au(111) Langmuir isotherm derived from experiments of ref 17. Our flat Au(111) surface isotherm also has a Langmuir shape. Obviously, the concentration range of adsorption derived from our simulations (of flat Au(111) as well as of NC) is orders of magnitude lower than the experimentally observed adsorption isotherm for SC8. From the work presented in this paper, we know that the range of adsorption is mainly determined by the interaction strength between Au and S. Using adsorption isotherm scaling (Appendix A), we estimate the Au−S interaction strength at $\epsilon/k_B \approx 1000$ K for the experimental isotherm instead of the value of $\epsilon/k_B \approx 2795$ K used in our simulations. This raises the question whether or not the Au−S interaction is really as strong as that modeled by Hautman and Klein,[20] Landman et al.,[28] and by us. A possible answer lies in the nature of the Au−S interaction. This interaction could either be a thiolate bond (formed by removal of the thiol hydrogen)[30] or physisorption of the thiol group to the gold surface. It is still unclear which of the possibilities prevails.[48] The thiolate adsorption energy was used to derive Au−S interaction potentials in previous simulations (for example, in refs 20 and 28). This interaction is three to four times as strong as that for the thiol−gold interaction.[30] Assuming that the SC8 adsorption measurements[17] are accurate, our adsorption isotherm scaling method suggests that monothiols are physisorbed to the Au(111) surface rather than chemisorbed.

4.1.3. Structural Properties of Adsorbed Systems with Explicit Solvent. In this section, we address the structural properties of thiol and solvent molecules in explicit solvent systems for a gold NC and a flat Au(111) surface. We consider two thiols of different chain length (SC4 and SC10) to address tail length effects. Furthermore, we investigate how the structure of the systems is affected by the loading. Therefore, we consider both surfactants at 30%, 60, and 100% of the maximum loading N_{max}. From *NVT* simulations of Au NCs and Au slabs, (partially) capped by thiols in solution, we determined the average orientations of the thiol chains with respect to the Au surface. The solvent structure was analyzed using the radial distribution function $g(r)$ of the solvent, with r as the distance from the center of an hexane molecule to the center of the NC or the gold slab.

We determined the orientations of the system components as follows. For each molecule, we defined the vector $\mathbf{r}$ that connects the first segment to the last. Furthermore, for each molecule, we calculated the vector $\mathbf{r}'$ that connects the NC center of mass to the molecule center of mass. For systems containing a gold slab, $\mathbf{r}'$ is simply the vector $\hat{\mathbf{z}}$ normal to the surface We subsequently determined the distribution $P(\alpha)$ of the minimal angle $\alpha \in [0,90°]$ between $\mathbf{r}$ and $\mathbf{r}'$. Low values of α represent chains that are oriented perpendicular to the surface, whereas $\alpha \rightarrow 90°$ represents chains that are oriented parallel to the NC or the flat Au(111) surface.

The orientational distributions of thiols on NCs are shown in Figure 11. At low loading, the distributions $P(\alpha)_{SC4}$ of the adsorbed SC4 thiols is almost random. $P(\alpha)_{SC4}$ shifts to lower angles α by increasing the loading to 60%. At the highest loading, the distribution $P(\alpha)_{SC4}$ is peaked at low angles α, indicating that most of the thiol chains are oriented perpendicular to the NC surface. The average orientation of the longer-chain thiols (SC10; see Figure 11) changes less as a function of loading (see also the right panel of Figure 11). As our NC is quite small, there is simply not enough space on the surface to accommodate for thiol chains lying parallel to the surface as one would expect for flat Au(111) surfaces.

In Figure 12, we show the thiol orientational distributions $P(\alpha)$ for flat Au(111) surfaces at various coverages for SC4 and SC10 in hexane. We observe that while SC4 molecules homogeneously become more upright with increasing coverage,

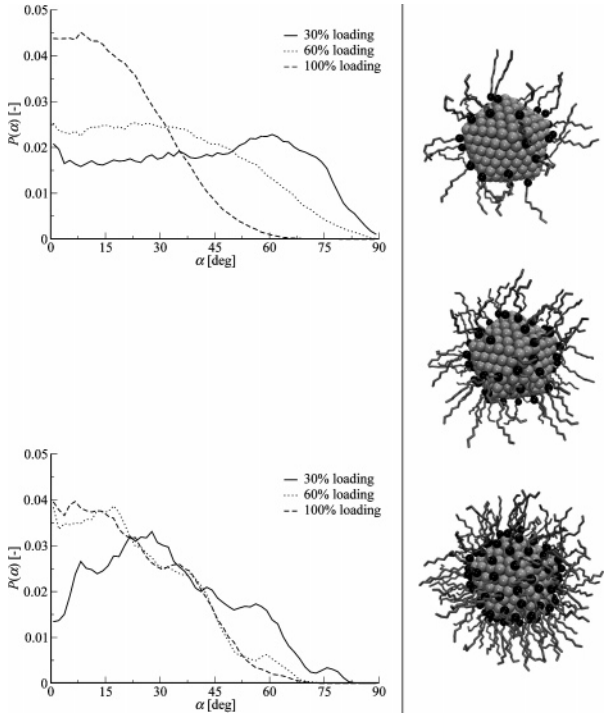

Figure 11. Thiol orientational distributions for alkyl thiol−hexane systems as a function of loading a Au_{561} NC. Top-left: SC4 system. Bottom-left: SC10 system. The right panel shows simulation snapshots taken from the SC10 simulations at increasing loading (from top-right to bottom-right).

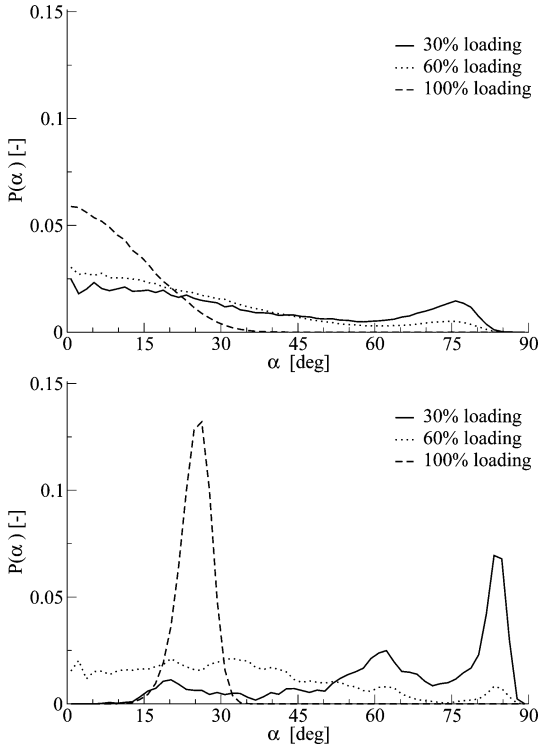

Figure 12. Orientational distributions of the thiol in alkyl thiol−hexane systems with a gold (111) slab at various surface coverages. Top: SC4; Bottom: SC10. Maximum loading with thiols is $N_{max} = 96$.

SC10 molecules strongly prefer to lie parallel to the Au surface at low coverages, and at full coverage (SAM regime), they have a 26° angle with the surface normal, on average (see Figure 12).

Evidently, long-chain thiols have a higher degree of configurational freedom compared to the short-chain thiols. Therefore, they can lie flat on the Au(111) surface more easily than short-chain thiols. For this reason, at low loadings, the SC10 molecules already occupy the Au surface almost completely, and SC4 molecules do not.

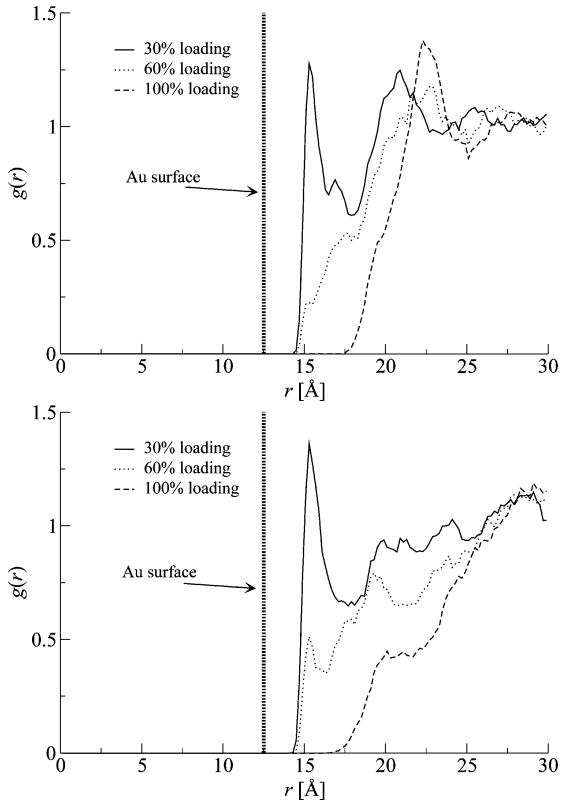

Figure 13. Solvent radial distribution functions $g(r)$ between the NC center of mass and the center of the hexane molecule for alkyl thiol−hexane systems with a Au_{561} NC at $T = 300$ K. Top: SC4 system. Bottom: SC10 system.

The solvent structural data for the NC (SC4 and SC10) are shown in Figure 13. At low and intermediate loadings of both SC10 and SC4, the first shell of solvent molecules is present near the Au surface, at regions where there are no thiols. Here, a large fraction orients itself parallel to the Au surface, maximizing the favorable interaction with gold. At high loadings, these vacant sites are occupied by thiols, and therefore, the first *n*-hexane solvation shell is shifted to larger distances *r*.

Figure 14 shows that, at low and intermediate loadings of SC4, there are some vacant regions on the flat gold (111) surface where solvent molecules are located. However, already at low SC10 loadings on flat Au(111), the surface is covered (almost) completely, leaving no room for solvents to reside near the Au surface. Therefore, the first peak of $g(r)$ at 30% loading for SC10 is low. By increasing the loading of SC4 or SC10 surfactants, the SAM becomes impenetrable for solvent molecules, and thus, the first solvation shell is shifted to a larger *r*.

4.2. Selective Adsorption to Au NCs and Au(111) Surfaces. To investigate the composition of coadsorbed alkyl thiols, we carried out simulations of binary thiol mixtures adsorbed on gold in the presence of the explicit solvent (*n*-hexane) for both a flat Au(111) surface and a NC. We compare the results to those from simulations without solvent. The total number of thiol molecules is kept fixed. Identity changes between different thiols are performed (semi-grand-canonical MC). During simulations with explicit solvent, we also allowed for solvent molecule exchange moves with the solvent reservoir (see Figure 1), but we did not allow for identity changes between solvents

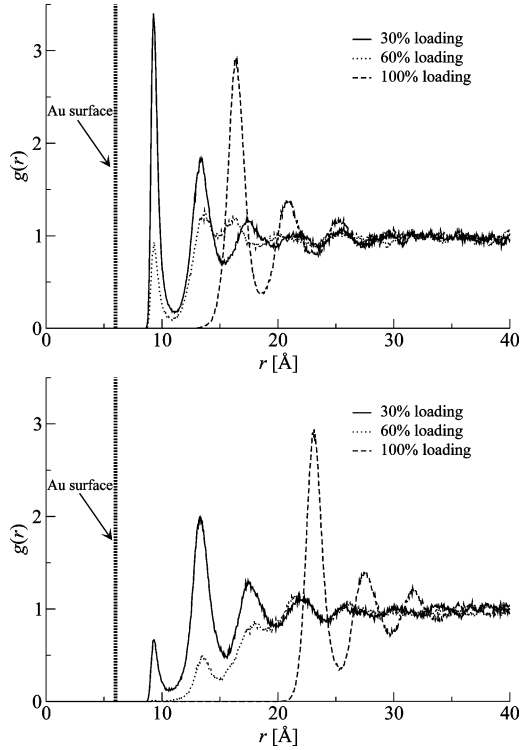

Figure 14. Solvent radial distribution functions $g(r)$ between the flat Au(111) substrate and the center of the hexane molecule for alkyl thiol−hexane systems with a gold (111) slab at various surface coverages and $T = 300$ K. Top: SC4 system. Bottom: SC10 system.

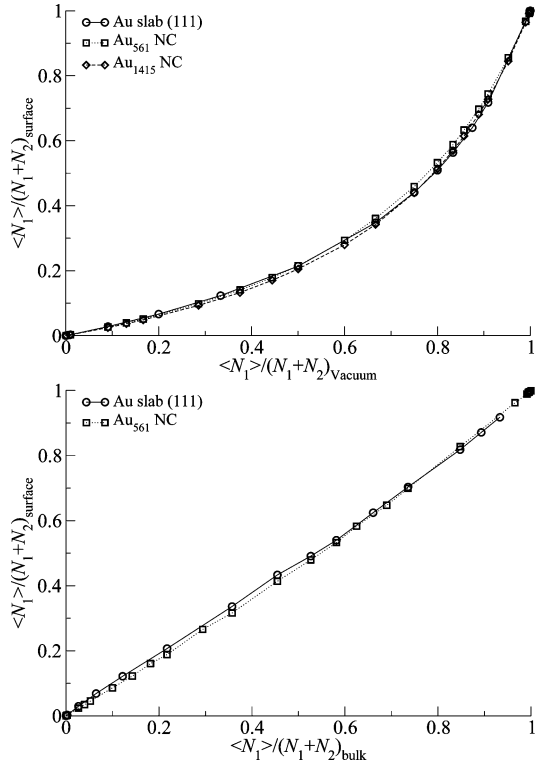

Figure 15. Adsorption selectivities for SC3−SC4. Top: results from vacuum simulations. Bottom: results from simulations with explicit solvent. Error bars are smaller than the symbol size.

and surfactants. We discuss the following mixtures: SC3−SC4, SC3−SC7, SC9−SC10, and SC9−SC11.

Shevade et al.[24] performed similar simulations in which they assumed that the alkyl thiol solubility does not significantly change as a function of chain length, a situation resembling vacuum conditions. However, in Figure 2, we showed that the Henry coefficient of thiols in *n*-hexane increases exponentially with the tail length, and this will influence the selectivity. We performed simulations with and without solvent to assess solvent effects.

For the system containing the gold structure, we computed the average number of shorter-chain thiols (type 1) and longer-chain thiols (type 2), $\langle N_1 \rangle$ and $\langle N_2 \rangle$, respectively, as a function of the ratio of their fugacities f_1 and f_2 from the simulation data. This ratio was converted to the concentration ratio $\langle N_1 \rangle / (\langle N_1 \rangle + \langle N_2 \rangle)$ for the other simulation box according to the procedure outlined in section 3. To investigate how the size of the NC affects selective adsorption, we studied two NCs, Au_{561} and Au_{1415}, which have $N_{max} = 124$ and 212 adsorbed thiols at their surfaces, respectively. The simulations with flat Au(111) surfaces were also performed at full coverage ($N_{max} = 96$ thiol molecules, arranged in a hexagonal overlattice).

The results are shown in Figures 15−18. In vacuum, the longer-chain thiol is always preferred over the shorter-chain one. This effect is more pronounced for longer alkyl chains and increases with the difference in chain length.[24] For an explanation, we refer to Figure 1. When a thiol molecule is transferred from the ideal gas reservoir to the system with a gold structure, it gains energy from interactions with gold and from Van der Waals interactions between carbon tails. This energy gain is larger for longer-chain thiols, and therefore, they are preferably adsorbed. The difference in these energy gains is the driving force for selectivity. On Au(111), the surfactants are ordered and adopt a tilted configuration, while on a NC, this tilted

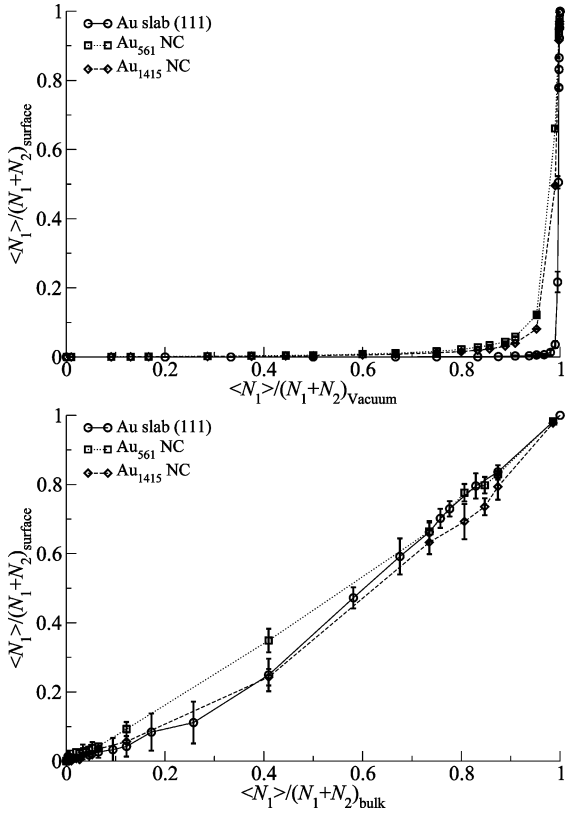

Figure 16. Adsorption selectivities for SC3−SC7. Top: results from vacuum simulations. Bottom: results from simulations with explicit solvent.

structure is frustrated and destroyed by the convex shape of the NC. This frustration becomes less for larger NCs. Therefore, the selectivity is strongest on the flat (111) surface and least on

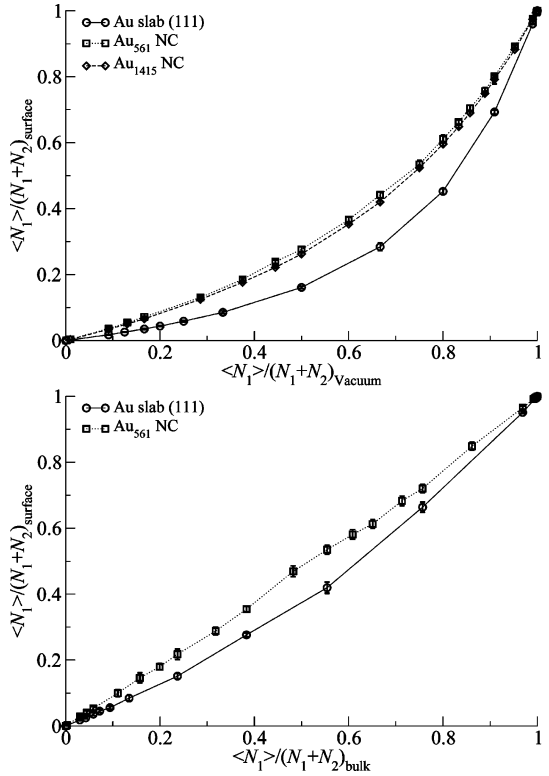

Figure 17. Adsorption selectivities for SC9−SC10. Top: results from vacuum simulations. Bottom: results from simulations with explicit solvent.

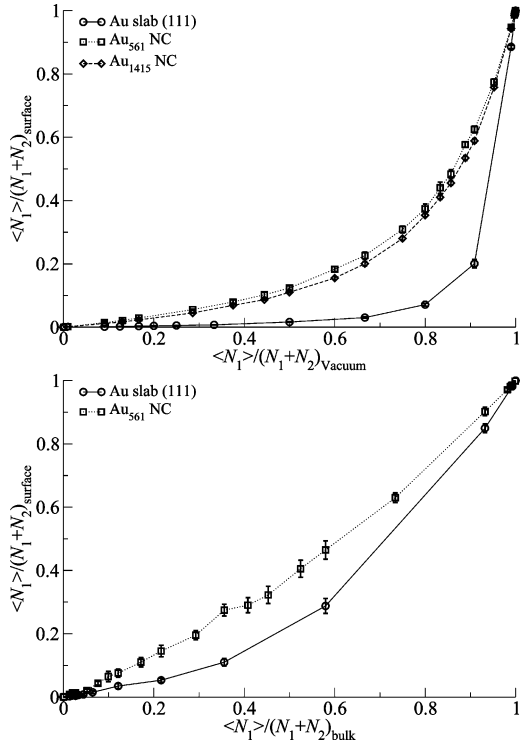

Figure 18. Adsorption selectivities for SC9−SC11. Top: results from vacuum simulations. Bottom: results from simulations with explicit solvent.

the small NC (compare the curves for Au_{561} and Au_{1415} NCs in Figures 15−18).

The situation is crucially different for systems with explicit solvent. Longer-chain thiols are again preferred over the shorter chains on a flat Au(111) surface, but the effect is much less pronounced than in vacuum. On NCs, selectivity is hardly present at all. To understand this, see Figure 1. We have to consider an exchange of a thiol from the bulk solution to the system with a gold structure and compare the energetic gains for two thiol types. These gains originate from interactions with gold and from Van der Waals attraction of aliphatic chains, but they are accompanied by the loss of attractive solvent−gold and solvent−thiol interactions. Gold−thiol interaction are almost identical for both thiol types and hence not significant for selectivity. Aligned tails on a flat surface have a stronger effective interaction than they would have in a solution, and this difference increases with chain length. On a NC, tails do not benefit from the arrangement in this way. Therefore, only tail−tail interactions between alkyl thiols on the flat (111) surface have a significant contribution to the difference in energetic gains. This explains why NCs show almost no selectivity and the selectivity on flat (111) surfaces is weaker than that in vacuum.

Our simulation results show that a solvent plays a large role in the selective adsorption of alkyl thiols to gold structures. Such solvent effects have previously[24] been overlooked. For the exchange of thiol capping layers on NCs, the key property to adjust is the concentration ratio of two thiol types in solution, not so much the chain length. Another possibility would be to use surfactants with different head groups. Exchange will then be observed if the two head groups exhibit different adsorption behavior.

5. Conclusions

Our adsorption studies show that the solvent plays an important role in the thermodynamic properties of thiol monolayers on both flat (111) gold surfaces and NCs. Two major solvent effects are (1) competitive adsorption between surfactants and solvents and (2) reduction of attractive interactions between aliphatic tails. Moreover, the phase behavior of unsaturated monolayers of long-chain thiols changes in the presence of a solvent. Therefore, phenomena observed in vacuum may be different from those observed in solution; in the latter case, the solvent cannot be neglected in computer simulations.

Our studies of the structure of the capping layer confirm that alkyl thiols SC*x* adopt a tilted confirmation in SAMs on planar gold (111) for $x > 6$, while capping layers of SC*x* on nanocrystals are conformationally disordered for $x < 12$.

On the NC surface, there is more space between aliphatic tails, which leads to weaker interactions and allows for a stronger interpenetration of the capping layer. This reduces the adsorption selectivity of thiol mixtures compared to that of the gold (111) surface and to vacuum.

Acknowledgment. T.J.H.V. acknowledges The Netherlands Organization for Scientific Research (NWO-CW) for financial support through a VIDI grant.

Appendix

A. Adsorption Isotherm Scaling. *A.1. Motivation.* Since the Au−S interaction is orders of magnitude stronger than other interparticle interactions, it seriously frustrates grand-canonical MC simulations. Simulations with a lower value for ϵ_{Au-S} would alleviate these simulations and thus increase computational efficiency significantly. Therefore, it is important to investigate whether or not the overall adsorption features depend on the precise value of ϵ_{Au-S} and whether or not it is possible to relate adsorption isotherms calculated for various values of ϵ_{Au-S}.

A.2. Statistical Mechanical Basis. We perform our simulations in the grand-canonical ensemble with the partition function

$$\Pi(\mu VT) = \sum_{N=0}^{\infty} \exp[\beta\mu N] \times Q(NVT) \tag{6}$$

where

$$Q(NVT) = \frac{1}{\Lambda^3 N!} \int \mathrm{d}x^N \mathrm{d}y^N \mathrm{d}z^N \exp[-\beta U(x^N, y^N, z^N)] \tag{7}$$

is the canonical partition function. Consider the following assumptions: (1) Chains are adsorbed to a surface in a single layer; (2) the main contribution to Q originates from the adsorption of sulfur segments; and (3) mutual interactions between thiols mainly depend on their distances in the direction parallel to the surface. Consider the sorbend as a slab in the xy plane. Using these assumptions, the potential energy U can be split into an adsorption part U_{ads} and a part containing sorbate−sorbate interactions U_{int}

$$U_{\mathrm{pot}}(x^N, y^N, z^N) = U_{\mathrm{ads}}(z^N) + U_{\mathrm{int}}(x^N, y^N) \tag{8}$$

We can then rewrite the partition function as

$$\Pi = \sum_{N=0}^{\infty} \exp[\beta\mu N] \times \frac{1}{\Lambda^{3N} N!} \times \int_{\Gamma_3} \mathrm{d}V^N \exp[-\beta U_{\mathrm{ads}}(z^N) - \beta U_{\mathrm{int}}(x^N, y^N)]$$

$$= \sum_{N=0}^{\infty} (I_{\mathrm{ads}} \exp[\beta\mu])^N \times \int_{\Gamma_2} \mathrm{d}x^N \mathrm{d}y^N \exp[-\beta U_{\mathrm{int}}(x^N, y^N)] \tag{9}$$

where dV is short for dxdydz, Γ_2 and Γ_3 are the 2− and 3−dimensional configuration spaces, respectively, and I_{ads} is the integral over the box length B_z in the z direction

$$I_{\mathrm{ads}} = \int \mathrm{d}z \exp[-\beta U_{\mathrm{ads}}(z)] \tag{10}$$

I_{ads} can be considered as the adsorption affinity as it represents the shift in chemical potential caused by the adsorption energy. Assume that we simulate two systems with different adsorption potentials yielding shifts $I^{(1)}$ and $I^{(2)}$. From the last line of eq 9, it follows that the first system at chemical potential $\mu^{(1)}$ is equivalent to the second system at the chemical potential $\mu^{(2)}$

$$\mu^{(2)} = \mu^{(1)} + \frac{1}{\beta} \ln \frac{I^{(1)}}{I^{(2)}} \tag{11}$$

For a system of noninteracting particles on a flat surface, the second integral in eq 9 can be solved analytically. This leads to an exact expression for the adsorption isotherm

$$\langle N \rangle = \frac{1}{\beta} \frac{\partial \ln \Pi}{\partial \mu} = \Lambda^{-3} A I_{\mathrm{ads}} \exp(\beta\mu) \tag{12}$$

where A is the area of the adsorbing surface. For potentials relevant to our work, we can derive expressions for I_{ads} as a function of the interaction strength. Throughout this paper, we mapped our pair Au−SH and Au−CH_x interactions to the Hautman−Klein effective potential. By taking the second-order Taylor expansion around the position of the potential minimum z_{m}, we obtain a harmonic potential

$$V_{\mathrm{harm}}(z) = U_{\mathrm{m}} + \frac{1}{2} k_{\mathrm{harm}} (z - z_{\mathrm{m}})^2 \tag{13}$$

where U_{m} is the potential well depth, k_{harm} the harmonic force constant, and z_{m} the position of the potential well. For the Hautman−Klein potential (eq 3), U_{m} is related to k_{harm}, and the analytical solution of eq 10 yields

$$I_{\mathrm{ads}}^{\mathrm{harm}} = \exp[-\beta U_{\mathrm{m}}] \sqrt{\frac{2\pi}{\beta k_{\mathrm{harm}}}} = \exp[-\beta U_{\mathrm{m}}] z_{\mathrm{m}} \sqrt{\frac{1}{-\beta U_{\mathrm{m}}}} \sqrt{\frac{2\pi}{c}} \tag{14}$$

in which the proportionality constant c follows from k_{harm}. Equation 14 suggests a general form for the adsorption affinity

$$I_{\mathrm{ads}} \propto \exp[-\beta U_{\mathrm{m}}] \left(\frac{1}{-\beta U_{\mathrm{m}}} \right)^{\alpha} \tag{15}$$

with the exponent α close to 0.5. For the Hautman−Klein effective potential $U(z)$, we found, by numerical integration and fitting of I versus $-\beta U_{\mathrm{m}}$

$$I_{\mathrm{ads}}^{\mathrm{HK}} \propto \exp[-\beta U_{\mathrm{m}}] \left(\frac{1}{-\beta U_{\mathrm{m}}} \right)^{0.55} \tag{16}$$

where C_{12}, C_3, and z_0 are contained in the proportionality constant.

A.3. Monte Carlo Simulations. We computed adsorption isotherms for SC3 on a gold (111) slab with explicit atoms at $T = 300$ K for various values of $\epsilon_{\mathrm{Au-S}}$. The resulting isotherms are plotted in Figure 19 (top). We found that at $T = 300$ K, the minimum of the effective Au−S interaction is $U_{\mathrm{m}} = -4.42\epsilon_{\mathrm{Au-S}}$. This allowed us to rescale the isotherms according to eqs 11 and 16. Figure 19 (bottom) shows that, indeed, all isotherms collapse.

For the same thiol (SC3), we determined adsorption isotherms on a Au_{561} NC at $T = 300$ K for $\epsilon_{\mathrm{Au-S}}/k_B$ ranging from 1000 to 4260 K. The raw adsorption isotherms as well as the scaled isotherms (to $\epsilon_{\mathrm{Au-S}}/k_B = 4260$ K) are plotted in Figure 20. From the simulation data, we found that $U_{\mathrm{m}} \approx -4.28\epsilon_{\mathrm{Au-S}}$. This value is slightly lower for the flat (111) surface, as the number of Au−S interactions is larger for the flat (111) surface compared to that for a NC surface. We verified that the above scaling relation (eqs 11 and 16) and its associated scaling factor are exactly the same in simulations with explicit solvent (both for the NC and the flat Au(111) surface systems).

We conclude that the isotherm scaling as predicted by eq 11 can correctly describe the adsorption of thiols to a gold (111) surface or NC. Thus, the shape of an adsorption isotherm is determined by mutual interactions between thiols, and its adsorption range is determined by the gold−sulfur interactions.

B. Biased Insertion Technique. Biased insertion can significantly improve the efficiency of conventional grand-canonical MC. Two possible ways to realize this are often used, (1) generate F trial positions randomly for the first bead and select one of them with a probability proportional to its Boltzmann weight[49] and (2) insert the first bead at a trial position (x', y', z') with a probability proportional to a predefined distribution $\rho(x, y, z)$.[50] The latter is useful only if favorable positions for particles are known a priori. In our case, thiol heads stay preferably close to the gold surface. We combine the two methods by generating F trial positions for the first bead according to a certain distribution $\rho(x, y, z)$ and then selecting one of them with a

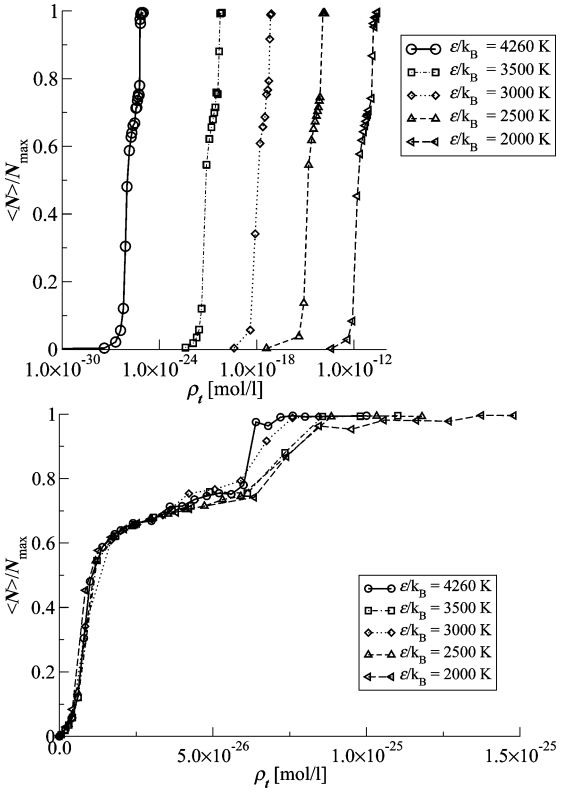

Figure 19. Adsorption isotherms of SC3 to a flat Au surface with explicit atoms (no solvent). Top: adsorption isotherms determined for different Au−S interaction strengths ($2000 \leq \epsilon_{LJ}/k_B \leq 4260$ K). Bottom: adsorption isotherms (no solvent) for lower ϵ values scaled to $\epsilon/k_B = 4260$ K using eqs 11 and 16.

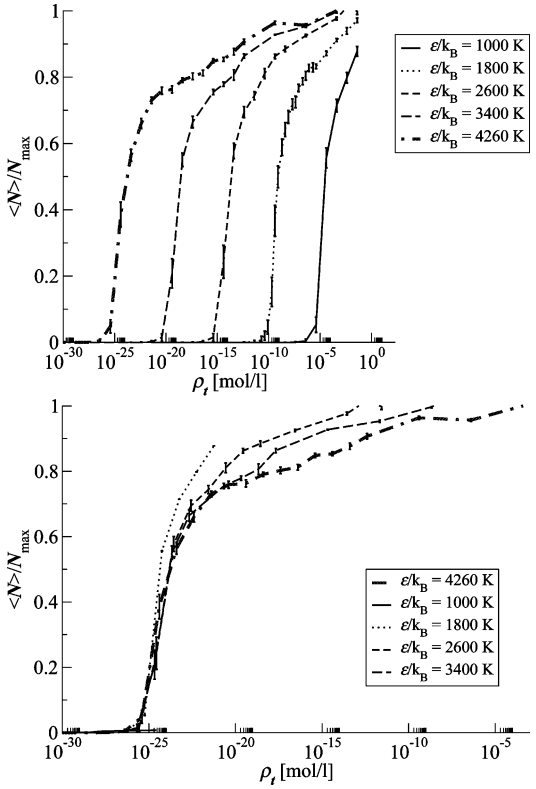

Figure 20. Top: adsorption isotherms of SC3 to a Au_{561} NC surface with explicit atoms (no solvents) determined for different Au−S interaction strengths $1000 \leq \epsilon_{LJ}/k_B \leq 4260$ K. Bottom: the same isotherms scaled to the $\epsilon/k_B = 4260$ K isotherm.

probability proportional to its Boltzmann weight. The arising bias is corrected in the acceptance rules. For insertion of a chain ($N \rightarrow N + 1$), the algorithm works as follows: (1) Generate F trial positions for the first bead according to the distribution $\rho(x, y, z)$ and compute their energies $U(1)$, ..., $U(F)$; (2) select one of them, n, with probability

$$P_{\text{ins}}^{\text{sel}} = \frac{\exp(-\beta U(n))}{\sum_{j=1}^{F} \exp(-\beta U(j))}$$

and set

$$w_1^{\text{ext}} = \frac{\sum_{j=1}^{F} \exp(-\beta U(j))}{F}$$

(3) Continue with the conventional CBMC algorithm, as in refs 38−41 and 51; compute the Rosenbluth weight

$$W^{\text{ext}} = \prod_{k=2}^{m} w_k^{\text{ext}}$$

where k runs over the beads of the chain; and (4) accept the insertion with the probability

$$P_{\text{ins}}^{\text{acc}} = \min\left(1, \frac{w_1^{\text{ext}}}{V\rho(x_n, y_n, z_n)} \frac{\exp(\beta\mu)VqW^{\text{ext}}}{N+1}\right) \quad (17)$$

in which V is the volume of the box, μ is the chemical potential, and q is the kinetic contribution to the partition sum.

The removal of a chain ($N \rightarrow N - 1$) is almost equivalent. (1) The position of the first bead of the selected molecule becomes the first trial position. Generate $F - 1$ others according to the distribution $\rho(x, y, z)$ and compute the energies $U(1)$, $U(2)$, ..., $U(F)$. (2) Continue with the conventional CBMC algorithm (for an old configuration) and compute the Rosenbluth weight W^{ext}. (3) Accept the removal with the probability

$$P_{\text{rem}}^{\text{acc}} = \min\left(1, \frac{V\rho(x_1, y_1, z_1)}{w_1^{\text{ext}}} \frac{N}{\exp(\beta\mu)VqW^{\text{ext}}}\right) \quad (18)$$

To show that detailed balance is obeyed, we consider the case when the distribution ρ is discrete and the chain consists of a single particle. Assume that the simulation box is partitioned in M cubelets, and to each of these cubelets i, a certain probability ρ_i is assigned. Normalization of ρ yields

$$\sum_{i=1}^{M} \rho_i V_i = 1$$

where $V_i = V/M$ is the volume of the ith cubelet. Consider the old configuration with N particles and the new one with $N + 1$, and denote the probability of generating a new trial configuration by $\alpha(o \rightarrow n)$ and the acceptance probability by $P_{\text{ins}}^{\text{acc}}$, the statistical weights of the old and the new configuration in the grand-canonical ensemble by $N(o)$ and $N(n)$, respectively, and the flux of configurations by $K(o \rightarrow n)$. The position of the new particle is selected out of F trial configurations. The configuration set of the $F - 1$ not-selected positions is denoted by $\tilde{b}$. In general, there are infinitely many such configuration

sets. Denote the family of all possible configuration sets by B, and its members are indexed by b. Then, we can split the flux of configurations $o \rightarrow n$ into the sum of fluxes through all possible trial moves leading from state o to state n

$$K(o \rightarrow n) = \sum_{i=1}^{M} \sum_{b \in B} N(o)\alpha(o \rightarrow n|b|i) \times P_{\text{ins}}^{\text{acc}}$$

$$K(n \rightarrow o) = \sum_{i=1}^{M} \sum_{b \in B} N(n)\alpha(n \rightarrow o|b|i) \times P_{\text{rem}}^{\text{acc}} \quad (19)$$

Super-detailed balance[51] requires that all terms in these equations are equal. For the probabilities to perform a trial move, we can write

$$\alpha(o \rightarrow n|\tilde{b}|i_n) = P_{o\rightarrow n}^{\text{att}} \times P_{o\rightarrow n}^{\text{gen}}(\tilde{b}) \times P_{\text{ins}}^{\text{sel}} \times P_{o\rightarrow n}^{\text{cub}}(i_n)$$

$$\alpha(n \rightarrow o|\tilde{b}|i_o) = P_{n\rightarrow o}^{\text{att}} \times P_{n\rightarrow o}^{\text{gen}}(\tilde{b}) \times P_{\text{rem}}^{\text{sel}} \times P_{n\rightarrow o}^{\text{cub}}(i_o) \quad (20)$$

where $P_{o\rightarrow n}^{\text{att}}$ is the probability of attempting an insertion move, which is equal to $P_{n\rightarrow o}^{\text{att}}$; $P_{o\rightarrow n}^{\text{gen}}(\tilde{b})$ is the probability of generating the configuration set $\tilde{b}$ during an insertion attempt; and $P_{n\rightarrow o}^{\text{gen}}(\tilde{b}) = P_{o\rightarrow n}^{\text{gen}}(\tilde{b})/F$ is the probability of generating the configuration set $\tilde{b}$ during a removal attempt. The permutation factor $1/F$ comes from the fact that in the removal algorithm, the old position is always the first one, while during an insertion, any of the F trial positions may be selected.

- $P_{\text{rem}}^{\text{sel}} = 1$ as no selection bias is involved in the reverse move;
- $P_{o\rightarrow n}^{\text{cub}} = \rho_{i_n} V/M$ is the probability that the new position lies inside of the cubelet i_n, and
- $P_{n\rightarrow o}^{\text{cub}} = 1/M$ as no bias in the selection of a cubelet is involved in the reverse move.

Combining eqs 19 and 20 and applying super-detailed balance leads to eq 17. Equation 18 can be derived in an analogous way.

References and Notes

(1) Andres, R. P.; Bielefeld, J. D.; Henderson, J. I.; Janes, D. B.; Kolagunta, V. R.; Kubiak, C. P.; Mahoney, W. J.; Osifchin, R. G. *Science* **1996**, *273*, 1690−1693.

(2) Reincke, F.; Hickey, S. G.; Kegel, W. K.; Vanmaekelbergh, D. *Angew. Chem., Int. Ed.* **2004**, *43*, 458−462.

(3) Frenkel, D. *Nat. Mater.* **2006**, *5*, 85−86.

(4) Murray, C. B.; Sun, S.; Gaschler, W.; Doyle, H.; Betley, T. A.; Kagan, C. R. *IBM J. Res. Dev.* **2001**, *45*, 47−56.

(5) Badia, A.; Gao, W.; Singh, V.; Demers, L.; Cuccia, L.; Reven, L. *Langmuir* **1996**, *12*, 1262−1269.

(6) Zhang, H.; Edwards, E. W.; Dayang Wang, D.; Möhwald, H. *Phys. Chem. Chem. Phys.* **2006**, *8*, 3288−3299.

(7) Kiely, C. J.; Fink, J.; Brust, M.; Bethel, D.; Schiffrin, D. J. *Nature* **1998**, *396*, 444−446.

(8) Gutiérrez-Wing, G.; Santiago, P.; Ascencio, J. A.; Camacho, A.; José-Ymacamán, M. *Appl. Phys. A* **2000**, *71*, 237−243.

(9) Peng, X.; Manna, L.; Yang, W.; Wickham, J.; Scher, E.; Kadavanich, A.; Alivisatos, A. P. *Nature* **2000**, *404*, 59−61.

(10) Murphy, C. J. *Science* **2002**, *298*, 2139−2141.

(11) Talapin, D. V.; Shevchenko, E. V.; Murray, C. B.; Kornowski, A.; Förster, S.; Weller, H. *J. Am. Chem. Soc.* **2004**, *126*, 12984−12988.

(12) Ulman, A. *Chem. Rev.* **1996**, *96*, 1533−1554.

(13) Schreiber, F. *Prog. Surf. Sci.* **2000**, *65*, 151−256.

(14) Zhang, L.; Goddard, W.; Jiang, S. *J. Chem. Phys.* **2002**, *117*, 7342 − 7349.

(15) Poirier, G. E.; Tarlov, M. J. *J. Phys. Chem.* **1995**, *99*, 10966−10970.

(16) Poirier, G. E. *Langmuir* **1999**, *15*, 1167−1175.

(17) Karpovich, D. S.; Blanchard, G. J. *Langmuir* **1994**, *10*, 3315−3322.

(18) Wuister, S.; van Houselt, A.; de Mello Donegá, C.; Vanmaekelbergh, D.; Meijerink, A. *Angew. Chem., Int. Ed.* **2004**, *43*, 3029−3033.

(19) Fink, J.; Kiely, C. J.; Bethel, D.; Schiffrin, D. J. *Chem. Mater.* **1998**, *10*, 922−926.

(20) Hautman, J.; Klein, M. *J. Chem. Phys.* **1989**, *91*, 4994−5001.

(21) Siepmann, J.; McDonald, I. *Mol. Phys.* **1993**, *79*, 457−473.

(22) Siepmann, J.; McDonald, I. *Mol. Phys.* **1992**, *75*, 255−259.

(23) Siepmann, J.; McDonald, I. *Phys. Rev. Lett.* **1993**, *70*, 453−456.

(24) Shevade, A. V.; Zhou, J.; Zin, M. T.; Jiang, S. Y. *Langmuir* **2001**, *17*, 7566−7572.

(25) Mizutani, W.; Ishida, T.; Tokumoto, H. *Appl. Surf. Sci.* **1998**, *132*, 792−796.

(26) Ryu, S.; Schatz, G. C. *J. Am. Chem. Soc.* **2006**, *128*, 11563−11573.

(27) Mahaffy, R.; Bhatia, R.; Garrison, B. J. *J. Phys. Chem. B* **1997**, *101*, 771−773.

(28) Luedtke, W. D.; Landman, U. *J. Phys. Chem. B* **1998**, *102*, 6566−6572.

(29) Sellers, H.; Ulman, A.; Shnidman, Y.; Eilers, J. E. *J. Am. Chem. Soc.* **1993**, *115*, 9389−9401.

(30) Nuzzo, R. G.; Zegarski, B. R.; Dubois, L. H. *J. Am. Chem. Soc.* **1987**, *109*, 733−740.

(31) Luedtke, W.; Landman, U. *Faraday Discuss.* **2004**, *125*, 1−22.

(32) Schapotschnikow, P.; Pool, R.; Vlugt, T. J. H. *Comput. Phys. Commun.* [Online early access]. DOI:10.1016/j.cpc.2007.02.028.

(33) Lal, M.; Plummer, M.; Richmond, N. J.; Smith, W. *J. Phys. Chem. B* **2004**, *108*, 6052−6061.

(34) Marks, L. D. *Rep. Prog. Phys.* **1994**, *57*, 603−649.

(35) Ascencio, J. A.; Gutiérrez-Wing, G.; Espinosa, M. E.; Martín, M.; Tehuacanero, S.; Zorrilla, C.; José-Ymacamán, M. *Surf. Sci.* **1998**, *396*, 349−368.

(36) Wang, Y.; Teitel, S.; Dellago, C. *Chem. Phys. Lett.* **2004**, *394*, 257−261.

(37) Dubbeldam, D.; Calero, S.; Vlugt, T. J. H.; Krishna, R.; Maesen, T. L. M.; Smit, B. *J. Phys. Chem. B* **2004**, *108*, 12301−12313.

(38) Siepmann, J.; Frenkel, D. *Mol. Phys.* **1992**, *75*, 59−70.

(39) Frenkel, D.; Mooij, G.; Smit, B. *J. Phys.: Condens. Matter* **1992**, *4*, 3053−3076.

(40) de Pablo, J.; Laso, M.; Suter, U. *J. Chem. Phys.* **1992**, *96*, 6157−6162.

(41) Siepmann, J. Configurational-bias Monte Carlo: Background and Selected Applications. In *Computer Simulation of Biomolecular Systems: Theoretical and Experimental Applications*; van Gunsteren, W. F., Weiner, P. K., Wilkinson, A. J., Eds.; Escom Science Publisher: Leiden, The Netherlands, 1993; pp 249−264.

(42) Metropolis, N.; Rosenbluth, A.; Rosenbluth, M.; Teller, A.; Teller, E. *J. Chem. Phys.* **1953**, *21*, 1087−1092.

(43) Barker, J.; Watts, R. *Chem. Phys. Lett.* **1969**, *3*, 144−145.

(44) Martin, M.; Siepmann, J. *J. Am. Chem. Soc.* **1997**, *119*, 8921−8924.

(45) Kofke, D.; Glandt, E. *Mol. Phys.* **1988**, *64*, 1105−1131.

(46) Lide, D. R., Ed. *Handbook of Chemistry and Physics*, 76th ed.; CRC press: Boca Raton, FL, 1995.

(47) Chandler, D. *Introduction to Modern Statistical Mechanics*, 1st ed.; Oxford University Press: New York, 1987.

(48) Grönbeck, H.; Curioni, A.; Andreoni, W. *J. Am. Chem. Soc.* **2000**, *122*, 3839−3842.

(49) Esselink, K.; Loyens, L. D. J. C.; Smit, B. *Phys. Rev. E* **1995**, *51*, 1560−1568.

(50) Snurr, R. Q.; Bell, A. T.; Theodorou, D. N. *J. Phys. Chem.* **1993**, *97*, 13742−13752.

(51) Frenkel, D.; Smit, B. *Understanding Molecular Simulations*, 2nd ed.; Academic Press: San Diego, CA, 2002.